JOURNAL OF PROPULSION AND POWER
Vol. 25, No. 3, May–June 2009

# Circumferential Film Cooling Effectiveness in a $LOX/H_2$ Subscale Combustion Chamber

R. Arnold,* D. Suslov,† and O. J. Haidn‡
*DLR, German Aerospace Center, Lampoldshausen, 74239 Hardthausen, Germany*

DOI: 10.2514/1.40305

**To study wall temperature distribution, film cooling effectiveness, and wall heat flux reduction due to film cooling in the circumferential direction, experimental investigations have been carried out, using gaseous hydrogen as a film coolant with tangential slot injection in close proximity to the injector face plate. A Vulcain-2-like test case has been performed, using a combustion chamber pressure up to 11.5 MPa at a high-mixture ratio of 6 with ambient temperatures of hydrogen. The experimental investigations have shown significant variations of wall temperatures due to injector design, as well as a distribution of film cooling effectiveness which persists far downstream from the film coolant injection slots. Circumferential variations of wall temperature and film cooling effectiveness are much more pronounced at higher combustion chamber pressures.**

## Nomenclature

| | | |
|---|---|---|
| $a$ | = | distance between two slots |
| $b$ | = | injection slot width, mm |
| $c_p$ | = | specific heat capacity for constant pressure, J/(kgK) |
| $d$ | = | distance from hot gas side, mm |
| $d, D$ | = | chamber, mm |
| $I$ | = | momentum flux ratio, – |
| $l_{\text{rec}}$ | = | recess length, mm |
| $M$ | = | film blowing rate, – |
| Ma | = | Mach number, – |
| $\dot{m}$ | = | mass flow rate, kg/s |
| $Pr$ | = | Prandtl number, – |
| $p$ | = | pressure, MPa |
| $\dot{q}$ | = | heat flux density, $W/m^2$ |
| $\dot{q}$ | = | averaged heat flux density, $W/m^2$ |
| $Re$ | = | Reynolds number, – |
| $s$ | = | injection slot height, mm |
| $T$ | = | temperature, K |
| Tu | = | turbulence level, – |
| $t$ | = | liquid oxygen post wall thickness |
| $t$ | = | time, s |
| $u$ | = | velocity, m/s |
| $x$ | = | distance downstream from point of film injection, mm |
| $\alpha$ | = | tapering angle, deg |
| $\beta$ | = | spreading angle, deg |
| $\gamma$ | = | angle of film coolant injection, deg |
| $\Delta\dot{q}$ | = | heat flux reduction, $W/m^2$ |
| $\Delta\Theta$ | = | variation of film cooling effectiveness, – |
| $\delta$ | = | boundary-layer thickness, mm |
| $\eta$ | = | adiabatic film cooling effectiveness, – |
| $\Theta$ | = | film cooling effectiveness, – |
| $\lambda$ | = | thermal conductivity, W/(mK) |
| $\mu$ | = | dynamic viscosity, kg/(ms) |
| $\xi$ | = | angle in injector triangle, deg |
| $\rho$ | = | density, $kg/m^3$ |

*Subscripts*

| | | |
|---|---|---|
| ad | = | adiabatic |
| cc | = | combustion chamber, hot gas, mainstream |
| $f$ | = | film cooling |
| $H_2$ | = | hydrogen |
| $i$ | = | inner |
| max | = | maximum |
| min | = | minimum |
| $O_2$ | = | oxygen, liquid oxygen |
| $o$ | = | outer |
| tot | = | total |
| $W$ | = | wall |
| 0 | = | without film cooling |
| 2 | = | film at point of injection |

## I. Introduction

IN ADDITION to an increase in engine reliability, an enhancement of the specific impulse and thrust are the main objectives for next-generation rocket propulsion systems [1,2]. Because the combustion chamber pressure is the driving parameter for engine size, these ambitious goals can only be realized with higher combustion chamber pressure, which simultaneously results in a considerable increase of structural and thermal loads. A higher combustion pressure $p_{\text{cc}}$ causes an almost linear increase of the heat flux level $\dot{q}$ to the wall [1,3]:

$$\dot{q} \propto p_{\text{cc}}^{0.8} \tag{1}$$

Large temperature differences between the hot gases and the combustion chamber liner in conjunction with combustion pressures in typical high performance engines [for example, space shuttle main engine (SSME) $p_{\text{cc}} = 19$ MPa [4], RD-170 (RD: Russian expression for rocket engine): $p_{\text{cc}} = 25$ MPa [5], RD-0120: $p_{\text{cc}} = 22$ MPa [5]] result in extreme heat flux levels and temperature gradients through the combustion chamber. Because of high chamber pressures, hot gas side liner walls in current rocket engines are exposed to heat fluxes exceeding 100 $MW/m^2$ (SSME, RD-170, RD-0120) and hot gas temperatures exceeding 3800 K in combination with a high mixture ratio ROF (mixture ratio oxidizer/fuel) [4,5]. Active protection of the liner materials, like CuAgZr (SSME), CuCr (RD-170), and CuCrZr (RD-0120) [6], from the impact of the hot combustion gases and the associated low-cycle fatigue is

Presented as Paper 5242 at the 44th AIAA/ASME/SAE/ASEE Joint Propulsion Conference and Exhibit, Hartford, CT, 21–23 July 2008; received 7 August 2008; revision received 20 November 2008; accepted for publication 30 November 2008. 

*Ph.D. Student, Institute of Space Propulsion; richard.arnold@dlr.de. AIAA Member (Corresponding Author).
†Research Engineer, Institute of Space Propulsion; dmitry.suslov@dlr.de.
‡Head of Technology, Institute of Space Propulsion; oskar.haidn@dlr.de. Associate Fellow AIAA.

necessary to provide safe and reliable operating of the rocket combustion chamber.

With regenerative cooling, turbopumps and turbines are heavily loaded because of the pressure drop in cooling channels, which results in limitations of engine lifetime, reliability, and safety margins. For example, to provide a chamber pressure of about 19 MPa in the SSME, preburner and turbopumps are operated at almost 40 MPa, which has a significant impact on the engine lifetime [7]. Furthermore, due to high structural loads, an increase of regenerative cooling is not possible by a further reduction of the wall thickness because of material inhomogeneity and manufacturing limitations. Improved regenerative cooling could only be accomplished by an increased Reynolds number of the propellant inside the cooling channels, which would give better heat transfer from the wall to the coolant, but which would also increase the pressure drop and propellant feed system loads.

To reduce regenerative cooling as well as the propellant feed system requirements, a number of film cooling related methods have been developed in the past for the protection of the hot gas side combustion chamber walls. Besides typical film cooling with the coolant injection through slots or orifices, in cases when a coaxial injector head is used, a reduced propellant mixture ratio ROF at the outer row of injector elements, either by an increasing of the fuel mass flow rate or a decreasing of the oxidizer flow, results in a decrease of the thermal wall loads (*injector trimming*). For example, in the SSME the outer coaxial elements run at a mixture ratio of 3, whereas the overall mixture ratio is about 6. An angling (*biasing*) of the liquid oxygen (LOX) posts of the outer injector elements away from the combustion chamber walls, which is also used in the SSME, results in an eccentricity of the fuel annulus and therefore a higher fuel mass flow rate on the outer side of the coaxial injector elements [8].

All methods, like coolant film injection and injector trimming and biasing, reduce the wall temperatures and improve injector-wall compatibility. However, the protection of the combustion chamber wall, using a reduced mixture ratio, either by the injection of a gaseous or liquid film, or by injector trimming or biasing, results in a loss in engine performance. Because excessive cooling causes unnecessary losses of specific impulse, circumstantial knowledge of the impact of the film coolant on the one hand, and temperature distribution inside the combustion chamber on the other hand, is of vital importance. A basic understanding of film cooling effectiveness and injector-wall interaction in the axial and circumferential directions are required to minimize engine performance losses and provide necessary wall protection.

## II. Experimental Setup

All experimental investigations described in this study have been performed at the European Research and Technology Test Facility P8 at DLR Lampoldshausen [9] using high-pressure subscale combustion chamber E [10].

### A. Subscale Combustion Chamber E

With subscale combustion chamber E (see Fig. 1), stable operation can be guaranteed for a chamber pressure up to $p_{cc} = 15$ MPa in combination with a very high propellant mixture ratio ROF. This combustion chamber covers the full operating range of the European Ariane 5 first-stage Vulcain 2 engine ($p_{cc} = 11.5$ MPa , ROF $= 7.2$ [11]) with an additional extension of this operating range.

Modular design of the experimental combustion chamber ensures a maximum of flexibility for varied experiments and chamber configurations. Subscale combustion chamber E features a cylindrical segment with an overall length of 200 mm and an inner diameter of 50 mm, and a nozzle segment with a throat diameter of 33 mm. Convective cooling of both segments is provided by water which is heated by streaming through axial-arranged cooling channels. In doing so, uniform cooling in the circumferential direction can be assured.

As an advanced feature, it is possible to rotate the cylindrical segment of the combustion chamber with an angular accuracy of about 0.5 deg relative to the injector head. In doing so, it is possible to measure a two-dimensional thermal field throughout the combustion chamber and describe circumferential behavior of wall temperature distribution and film cooling effectiveness [10,12].

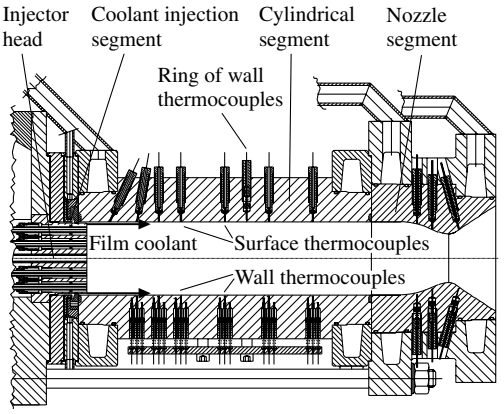


**Fig. 1 Subscale combustion chamber E.**

In the cylindrical segment, two rows of wall thermocouples are arranged in the axial direction in packages with three elements each with differing wall distances $d$ from the hot gas side. Based on the measured thermal gradient almost perpendicular to the chamber wall, it is possible to extrapolate the local surface temperatures with the use of a logarithmic function (*gradient method*) [10,13,14]. Furthermore, the application of one row of surface thermocouples provides a direct measurement of the local surface temperatures inside the combustion chamber.

In addition, for detailed investigation of circumferential film cooling effectiveness and injector-wall interaction with high angular accuracy, subscale combustion chamber E has been provided with a ring of 12 wall thermocouples with a constant wall distance $d =$ 1 mm (see Figs. 1 and 2). The axial position of the ring of thermocouples is located 112 mm downstream of the injector head face plate and film coolant injection position.

As a result of vibrations up to $100g$, and due to thermal material expansion and contraction during start, hot run, and shut down, there can appear to be liftoff and loss of mechanical contact of the thermocouple measurement point. A spring system provides a constant force to ensure reliable contact for all wall thermocouples during hot run tests (see Fig. 2) [13].

### B. Injector Head and Film Coolant Injection Segment

The injector head contains 15 coaxial injection elements, arranged in two different pitch circles with 10 elements in the outer, 5 in the inner circle, and a central torch igniter. The geometrical distribution is made in that way to get five identical injector triangles with one

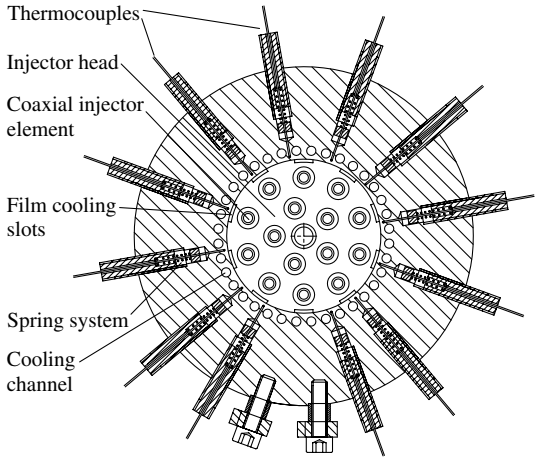


**Fig. 2 Ring of wall thermocouples in the cylindrical segment.**

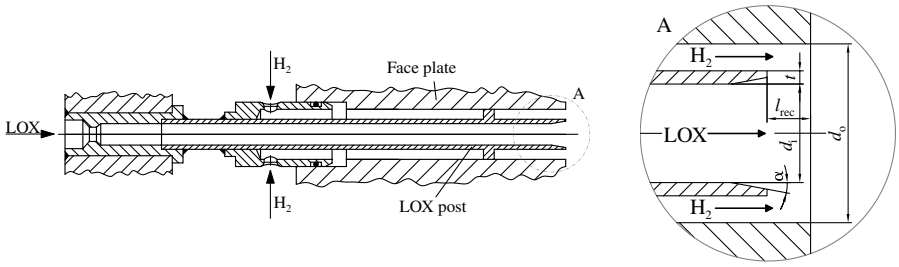


**a) Design of a coaxial injector element**

**b) Dimensions at the leading edge**

**Fig. 3 Coaxial injector element.**

coaxial element of the inner and two elements of the outer pitch circle (as shown later).

Figure 3 shows the engineering design of a single coaxial injector element as well as characteristic dimensions on the leading edge of the face plate (see Table 1). Liquid oxygen is fed into the LOX posts from a rear-mounted manifold, whereas the hydrogen is distributed by laterally arranged orifices.

For film cooling investigations, the injector head face plate is surrounded by a coolant injection segment (see Fig. 4). This segment provides 10 cooling slots evenly distributed in the circumferential direction, manufactured with high precision for tangential ($\gamma = 0$ deg) film coolant injection. Positions of these film cooling slots are consistent with the angular positions of the outer injector elements [10,15]. For each of the five identical injector triangles, the film coolant injection slots and outer coaxial injector elements are arranged in the angular positions $\xi = 0$ and $\xi = 36$ deg. The inner coaxial element is located at $\xi = 18$ deg, and symmetrical boundaries of the injector triangle are at $\xi = -18$ and $\xi = 54$ deg. Table 2 gives an overview of the film cooling slot geometry.

Because high-precision knowledge of the injected film temperature is essential for film cooling investigations, two thermocouples have been attached in the film injection segment to measure the film temperature just before the film coolant enters the combustion chamber. For future research investigations, it is possible to change slot geometry and slot number of the film coolant injection segment in a very easy way because of the modular design.

**Table 1 Data of the coaxial injector elements**

| | |
|---|---|
| Diameter ratio $d_o/d_i$, $H_2$/LOX, – | 1.67 |
| LOX post wall thickness, mm | 0.6 |
| Recess length $l_{rec}$, mm | 0 |
| Tapering angle $\alpha$, deg | 10 |

**Table 2 Data of the film coolant injection segment**

| | |
|---|---|
| Number of slots | 10 |
| Slot height $s$, mm | $0.4 \pm 0.015$ |
| Slot width $b$, mm | $3.5 \pm 0.015$ |
| Injection angle $\gamma$, deg | 0 |
| Distance between two slots $a$, mm | 12 |

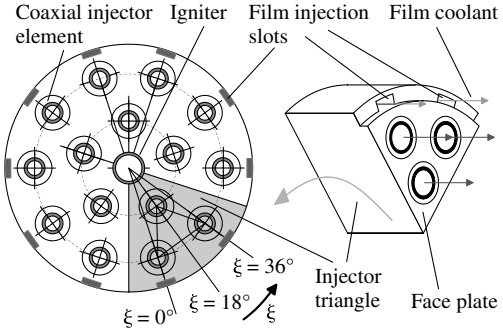


**Fig. 4 Injector head and film coolant injection segment.**

### C. Operating Conditions

For experimental investigation of circumferential temperature distribution and film cooling effectiveness in a high-pressure rocket combustion chamber, a typical test sequence has been generated, using LOX/$H_2$ as propellants [10,12]. Although the test facility P8 is capable of combustion chamber pressures up to about 25 MPa when using 50 mm subscale hardware, three major pressure intervals have been performed, giving real enginelike hot gas conditions on the one hand, with relatively moderate heat flux conditions on the other hand: 11.5 MPa (intervals 1–3), 8 MPa (intervals 4–6), and 5 MPa (intervals 7–9) with a constant mixture ratio ROF = 6 (see Table 3). Each pressure interval was divided into three sections with differing film coolant mass flow rates, which gave nine different operating conditions for each hot run. Table 3 gives an overview of the hot gas conditions, such as combustion chamber pressure $p_{cc}$, injector head propellant mass flow rates $\dot{m}_{H_2}$, $\dot{m}_{O_2}$, and propellant injection temperatures $T_{H_2}$ and $T_{O_2}$.

Notwithstanding typical injection temperatures of hydrogen in rocket engines such as SSME and Vulcain 2 ($T_{H_2} \approx 100$–$120$ K [1]), hydrogen at ambient temperature has been used for the present study. Ambient hydrogen is much easier to handle for first step experimental investigations compared to a cryogenic fluid and is suitable for obtaining a basic understanding of film cooling effectiveness and injector-wall interaction. Furthermore, in most empirical or semi-empirical film cooling models developed in the past by numerous authors, film coolant (mostly air) with ambient temperatures has been injected [16–19]. Comparability with existing film cooling models and the possibility of modeling ambient hydrogen as an ideal gas are further arguments for deviation from real enginelike parameters for the time being.

**Table 3 Hot gas conditions**

| Interval | 1 | 2 | 3 | 4 | 5 | 6 | 7 | 8 | 9 |
|---|---|---|---|---|---|---|---|---|---|
| $p_{cc}$, MPa | 11.9 | 11.8 | 11.6 | 8.3 | 8.2 | 8.0 | 5.2 | 5.1 | 5.0 |
| ROF, – | 6.02 | 6.00 | 5.99 | 5.99 | 5.99 | 5.99 | 5.99 | 5.99 | 5.99 |
| $\dot{m}_{H_2}$, kg/s | 0.60 | 0.60 | 0.60 | 0.42 | 0.42 | 0.42 | 0.26 | 0.26 | 0.26 |
| $\dot{m}_{O_2}$, kg/s | 3.62 | 3.61 | 3.61 | 2.51 | 2.51 | 2.51 | 1.58 | 1.58 | 1.58 |
| $T_{H_2}$, K | 287.9 | 285.5 | 283.1 | 278.8 | 278.4 | 277.3 | 277.1 | 276.2 | 274.9 |
| $T_{O_2}$, K | 113.5 | 111.5 | 111.2 | 112.8 | 113.3 | 113.2 | 114.8 | 115.2 | 115.6 |

**Table 4 Film cooling parameters**

| Interval | 1 | 2 | 3 | 4 | 5 | 6 | 7 | 8 | 9 |
|---|---|---|---|---|---|---|---|---|---|
| $\dot{m}_2/\dot{m}_{\text{tot}}$, % | 1.83 | 1.03 | 0 | 2.01 | 0.99 | 0 | 2.01 | 0.98 | 0 |
| $T_2$, K | 287.5 | 287.5 | —— | 288.3 | 289.2 | —— | 289.6 | 290.4 | —— |
| $M$, – | 2.85 | 1.61 | 0 | 3.13 | 1.56 | 0 | 3.15 | 1.56 | 0 |
| $u_2/u_{\text{cc}}$, – | 1.60 | 0.91 | 0 | 1.74 | 0.87 | 0 | 1.75 | 0.86 | 0 |
| $u_2/u_{\text{H}_2}$ | 0.94 | 0.52 | 0 | 1.07 | 0.53 | 0 | 1.08 | 0.53 | 0 |

Table 4 features a summary of investigated film cooling parameters like film blowing rate $M$, injection temperature $T_2$, and velocity ratio between hot gas and film coolant $u_2/u_{\text{cc}}$. As a reference for comparison with film cooling conditions and to identify the thermal footprints only due to the coaxial injector head without the influence of a film coolant, the last section of each pressure interval has been performed without the injection of a film coolant ($\dot{m}_2 = 0$ ).

## III. Film Cooling

Film cooling is a widely used cooling method for rocket engines to protect the combustion chamber walls from the impact of the hot combustion gases, not only at the position of the film injection but also farther downstream. It can be used either alone (e.g., in small engines for satellite propulsion) or in combination with regenerative cooling for very high heat fluxes, like it is applied among other engines in the Vulcain 2 of the European launcher Ariane 5, the SSME, or in the Russian RD-170-based family. For example, in the Vulcain 2 engine, film cooling is used in combination with the injector head and in the nozzle extension, where the turbine exhaust gases and the dump cooling is injected [20,21].

With the application of film cooling, a significant reduction of thermal and structural loads of the chamber walls as well as mechanical strains of the turbopumps because of the pressure drop in cooling channels can be obtained. Hence, the additional application of film cooling in combination with a regeneratively cooled liner wall in future high-pressure combustion chambers is the only possibility to improve safety and enhance lifetime and reliability. In doing so, it is fundamental to investigate the thermal heat load distribution, created by the injector design, and film cooling effectiveness, not only in the downstream direction but also circumferentially inside the combustion chamber to avoid hot spots and temperature asymmetry on the liner walls, which can cause serious limitations for engine operation.

### A. Film Cooling Effectiveness

Although there are a multitude of models describing film cooling effectiveness, mostly heat sink models which assume complete mixture of hot gas and coolant (for example, Tribus and Klein [22], Kutateladze and Leont'ev [23], and Goldstein and Haji-Sheikh [18]), most of them are not applicable in a high-pressure rocket combustion chamber. High temperature gradients inside the boundary layer and high combustion chamber pressures, turbulent flows, variable fluid properties of the hot gas and film coolant [e.g., $c_p = f(T)$], as well as recombination effects in close proximity of the chamber walls, giving an additional heat source, are not considered in existing film cooling models. In addition, all models given in literature are not designed for such high Reynolds numbers present in rocket combustion chambers.

In the literature, nondimensional adiabatic effectiveness $\eta$ is a widely used parameter to describe and compare film cooling results [16,18,23–27]. The difference between adiabatic wall temperature $T_{\text{ad}}$ and hot gas temperature $T_{\text{cc}}$ refers to the maximum difference between coolant temperature at injection point $T_2$ and hot gas temperature:

$$\eta = \frac{T_{\text{ad}} - T_{\text{cc}}}{T_2 - T_{\text{cc}}} \tag{2}$$

However, this definition of effectiveness cannot be applied in a typical copper alloy rocket combustion chamber due to the extreme high temperatures of the combustion gases and therefore extreme wall heat fluxes. Adiabatic wall temperatures would exceed safe operating temperatures of all known combustor materials. Hence, for a high-pressure combustion chamber, regenerative cooling and film cooling will be used in combination. Therefore, it is imperative to establish a different temperature ratio to describe film cooling effectiveness for a regenerative and film-cooled rocket combustion chamber. This new temperature ratio can be used as a measure of effectiveness for film cooling processes. The local temperature difference due to the application of film cooling will be compared with the maximal achievable temperature difference, where $T_{W,0}$ designates the wall temperature without, and $T_{W,f}$ the wall temperature with, film cooling:

$$\Theta(x) = \frac{T_{W,0}(x) - T_{W,f}(x)}{T_{W,0}(x) - T_2} \tag{3}$$

According to Eq. (3), a circumferential film cooling effectiveness $\Theta_\xi$ can be defined using the local temperature reduction between wall temperature without film cooling $T_{W,0}(\xi, x)$ and wall temperature with film cooling $T_{W,f}(\xi, x)$:

$$\Theta_\xi(x) = \frac{T_{W,0}(\xi, x) - T_{W,f}(\xi, x)}{T_{W,0}(\xi, x) - T_2} \tag{4}$$

In analogy to the description of the axial film cooling effectiveness [see Eq. (3)], Eq. (4) can be used to characterize film cooling effectiveness in the circumferential direction and the uniformity of the injected film, as well as the film spreading. It is essential for the development of thermally highly stressed rocket combustion chambers to minimize the circumferential variation of the wall temperature to avoid nonessential film mass flow rates. Local thermal hot spots on the chamber wall as a result of injector design or nonuniform film coolant injection can result in reduced engine lifetime and reliability, whereas increased cooling of the chamber wall due to high local variation of the thermal loads results in a loss of specific impulse and engine performance.

### B. Influence Parameters for Film Cooling Effectiveness

In general, film cooling effectiveness $\Theta$ is dependent on a multitude of geometrical (injection angle, slot height, slot width, and number of slots), fluidmechanical (blowing rate, ratios of momentum flux, boundary-layer thicknesses, and turbulence levels, and Reynolds numbers), and thermodynamical parameters (pressure, temperature, and ratios of pressure and temperature) [26,28,29]:

$$\Theta = f\left(\frac{x}{s}, M, \frac{T_2}{T_{\text{cc}}}, \frac{\rho_2}{\rho_{\text{cc}}}, \frac{\text{Tu}_2}{\text{Tu}_{\text{cc}}}, \gamma, \frac{c_{p,2}}{c_{p,\text{cc}}}, \frac{\mu_2}{\mu_{\text{cc}}}, \frac{\lambda_2}{\lambda_{\text{cc}}}, \frac{\delta_2}{\delta_{\text{cc}}}\right) \tag{5}$$

The blowing rate $M$ is a main parameter to characterize film cooling and describes the ratio of the mass velocity of the coolant to the hot gas stream mass velocity:

$$M = \frac{(\rho u)_2}{(\rho u)_{\text{cc}}} \tag{6}$$

In the past, experimental work has shown a clear connection between blowing rate and film cooling effectiveness for $M \leq 1$ as well as for $M > 1$ [30–32]. An increase of the blowing rate $M$ up to $M \approx 3$ indicates a better film cooling effectiveness for tangential slot

injection. This also applies for foreign gas injection in place of the well-examined test case of air injected into air.

## IV. Experimental Results

The experimental results consist of wall temperature distributions in the circumferential direction, film cooling effectiveness relative to an injector triangle, and circumferential and axial heat flux distributions.

### A. Circumferential Wall Temperature Distribution and Injector-Wall Interaction

The circumferential temperature distribution inside the combustion chamber wall material has been investigated to obtain information about the uniformity of the propellant combustion and therefore the circumferential thermal load distribution generated by the coaxial injector head design. Assuming a uniform propellant injection and atomization behavior of all coaxial injector elements, a local maximum of the wall temperatures can be expected directly downstream of the angular positions of the outer coaxial injector elements (see Fig. 4). Figure 5 shows schematically the superposition of the single flames in an injector triangle and the expected wall temperature distribution $T(\xi)$ with maximum values at $\xi = 0$ and $\xi = 36$ deg, and a local minimum at the angular position of the inner coaxial injector element ($\xi = 18$ deg). Maximum hot gas temperature inside the single flames occurs downstream of the point of injection in the area of the flame axis, whereas, in the outer region of the flame, a lower combustion temperature predominates [33,34]. With a sufficiently dense arrangement of the coaxial injector elements, the flame impact of the inner coaxial injector elements on the wall temperature distribution can be neglected, and similar wall temperatures will be expected for the positions $\xi = -18$ (no inner coaxial injector element) and $\xi = 18$ deg (inner coaxial injector element) in the injector triangle (see Fig. 4).

By the use of the wall thermocouple ring (see Figs. 1 and 2), located at the axial position $x/s = 280$ , a detailed distribution of the circumferential wall temperature variation has been measured for the pressure intervals 11.5, 8, and 5 MPa at various film blowing rates $M$ (see Fig. 6). Experimental results show a very good agreement with the schematical description of the circumferential wall temperature distribution following Fig. 5 for the angular positions $\xi = 144$–$180$ deg and $\xi = 324$–$360$ deg. A shifting of 8–10 deg compared with the expected temperature maxima directly downstream the positions of the outer coaxial injectors occurs in the interval $\xi = 0$–$108$ deg. Nonuniform injection and atomization of the propellants as well as swirl effects inside the combustion chamber may shift the positions of the minimum and maximum wall temperatures and also give different levels of the local minimum and maximum wall temperature values. The application of a film ($M > 0$ ) results in a significant reduction of the wall temperature at all circumferential positions (see Fig. 6). However, maximum wall temperature can be seen at the angular positions downstream of the outer coaxial injector elements and film coolant injection slots independent from the injection of a film coolant. Circumferential temperature variation between local maxima and minima increases with the combustion chamber pressure and is much more pronounced at higher pressure levels. A relatively uniform temperature distribution with about 50 K variation between different local temperature maxima and minima, respectively, at the upper pressure interval of 11.5 MPa with hot gas temperatures of more than 3400 K indicates the nearly symmetrical injection and combustion behavior of the coaxial injector head. No experimental data have been available for the interval $\xi \approx 180$–$220$ deg.

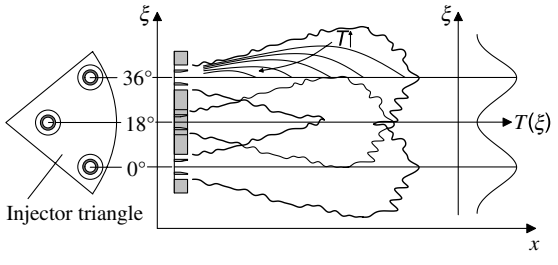


**Fig. 5 Superposition of single flame distribution.**

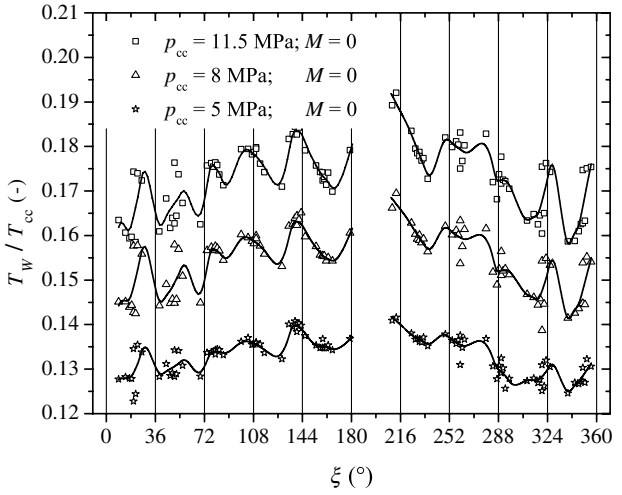


**a) No film cooling**

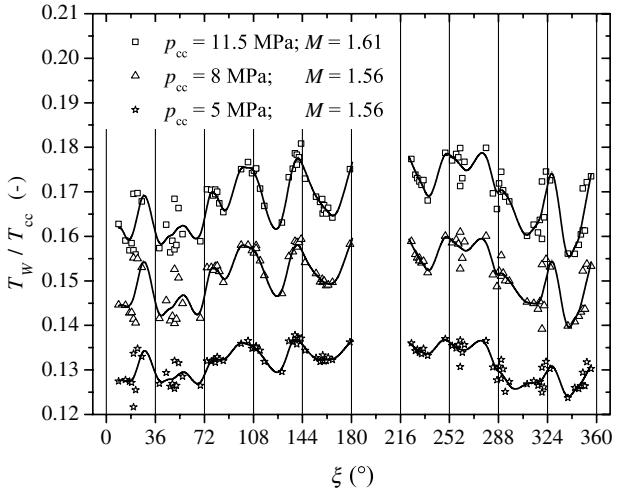


**b) Small film blowing rate**

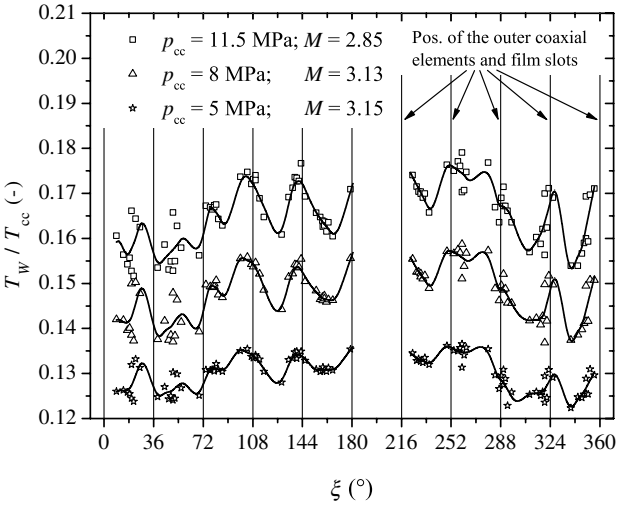


**c) High film blowing rate**

**Fig. 6 Circumferential wall temperature distribution ($d = 1$ mm, $x/s = 280$).**

Injector head induced nonuniform circumferential temperature distribution (see Fig. 6) results in a nonuniform heat flux variation and additional thermal and structural loads. These injector footprints can be observed inside subscale combustion chamber E from about 45 mm downstream of the propellant injection (see Fig. 7) and have been found ≈60 mm downstream of the face plate in engines like Vulcain 1 and Vulcain 2. With the implementation of film cooling in the proximity of the injector head, chemical impact of the hot combustion gases (oxygen and radicals like OH) on the chamber walls can be controlled. Besides a slight increase of the combustion chamber pressure of Vulcain 2 ($p_{cc} = 11.5$ MPa) compared to Vulcain 1 ($p_{cc} = 10.2$ MPa [35]), protection from chemical impact can be seen as a driving factor for the additional injection of a film coolant in the region of the face plate in Vulcain 2.

Statistical variability due to injector geometry, injection and propellant atomization, and combustion effects as well as thermocouple implementation can be reduced by averaging the experimental results presented in Fig. 6 and reducing them to a single injector triangle, which covers the angular interval $\xi = -18$–54 deg (see Fig. 4). Figure 8 shows the circumferential wall temperature distribution for the investigated pressure intervals $p_{cc} = 11.5$, 8, and 5 MPa. As mentioned earlier, local maximum wall temperature occurs straight downstream of the position of the outer coaxial injector element and film injection slot, whereas local minimum wall temperatures occur at the angular position of the inner coaxial injector element. Levels of the local minima at $\xi = -18$, 18, and 54 deg are the same order of magnitude with almost symmetrical temperature characteristics compared with the inner coaxial injector element. An influence of the inner coaxial injector element on the wall temperature distribution cannot be ascertained in the present investigation. Circumferential wall temperature variation as well as wall temperature reduction due to film cooling are much more pronounced at $p_{cc} = 11.5$ and 8 MPa in contrast to the lower pressure interval $p_{cc} = 5$ MPa.

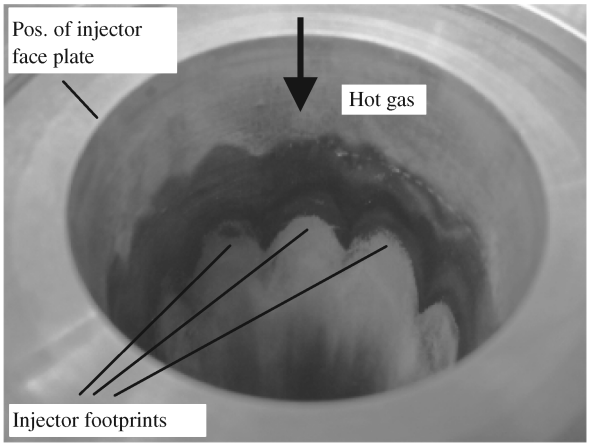


**Fig. 7 Injector footprints on chamber wall.**

### B. Circumferential Film Cooling Effectiveness

An essential issue in the development of thermally highly stressed rocket combustion chambers is the minimization of the circumferential wall temperature variation to avoid unnecessarily high film cooling mass flow rates. Local thermal hot spots on the chamber wall as a result of injector design or nonuniform film coolant injection can result in reduced engine lifetime and reliability, whereas increased cooling of the chamber wall will result in a loss of specific impulse and engine performance, as mentioned earlier.

The wall temperature reduction $\Delta T_W$ due to the application of film cooling is the first possibility for estimating the potency of the injected film coolant and judging the uniformity of the coolant spreading downstream of the injection:

$$\Delta T_W = T_{W,0} - T_{W,f} \tag{7}$$

Figure 9 presents the measured temperature reduction $\Delta T_W$ for the 11.5, 8, and 5 MPa pressure intervals. As expected, wall temperature reduction is directly proportional to the film cooling blowing rate $M$. However, the maximum temperature reduction occurs at the angular positions between the film coolant injection slots and not directly downstream of the coolant injection as might be expected. Temperature reduction of the 11.5 and 8 MPa intervals are of similar order of magnitude with a local temperature reduction $\Delta T_W \approx$ 10–45 K for the higher film blowing rate, and $\Delta T_W \approx$ 3–30 K for the lower blowing rate step.

For the combustion chamber pressure of 5 MPa, only marginal temperature reduction is achieved at this axial position with film cooling. Because of a much higher velocity ratio between propellant and oxidizer at the coaxial injector elements and a different atomization behavior compared with the considerably supercritical conditions at 8 and 11.5 MPa, as well as the much lower heat load, mixing of the film coolant and the hot gas likely occurs at a position more upstream and with less stratification effects. A clear connection between temperature reduction and angular positioning of coaxial

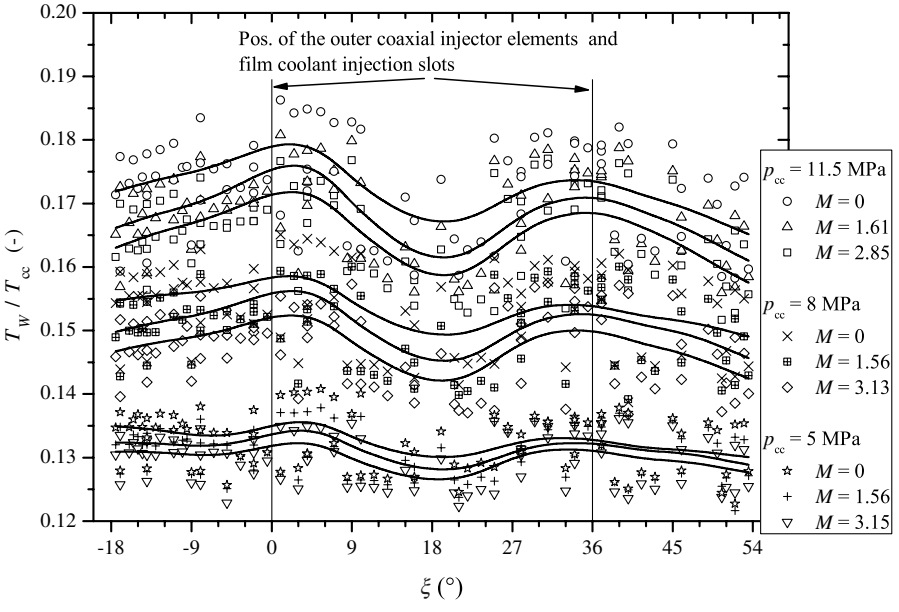


**Fig. 8 Circumferential wall temperature distribution relative to an injector triangle ($d = 1$ mm, $x/s = 280$).**

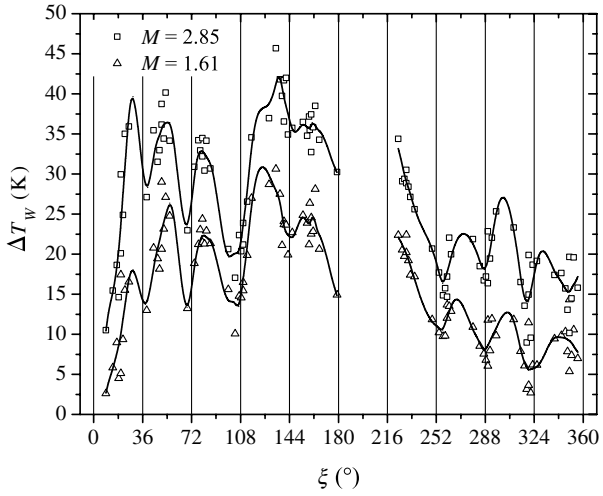


a) $p_{cc}$ = 11.5 MPa

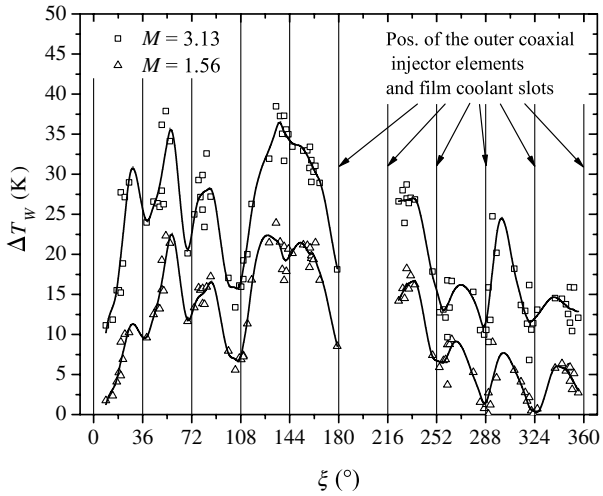


b) $p_{cc}$ = 8 MPa

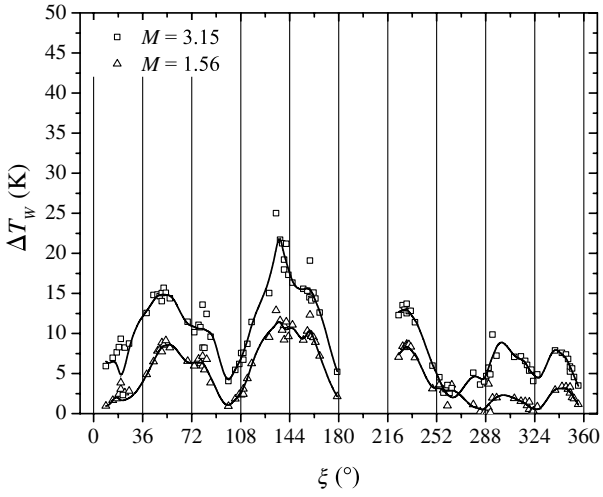


c) $p_{cc}$ = 5 MPa

**Fig. 9 Wall temperature reduction due to film cooling ($d = 1$ mm, $x/s = 280$).**

injector element and film coolant injection slot is only visible at certain angular positions (see Fig. 9).

The circumferential film cooling effectiveness presented in this study is based on measurements at a wall distance $d = 1$ mm due to the arrangement of the wall thermocouples in the thermocouple ring (see Figs. 1 and 2). Consequently, a higher local film cooling effectiveness has been measured compared with the film cooling effectiveness at a wall distance $d = 0$ on the hot gas side of the chamber surface.

The conversion of the measured circumferential film cooling effectiveness inside the chamber wall to the desired film cooling effectiveness on the combustion chamber surface can be done with the use of the wall heat flux densities inside the chamber wall without and with film cooling, $\dot{q}_{W,0}(\xi)$ and $\dot{q}_{W,f}(\xi)$, respectively (see Fig. 10):

$$T_{W,0}(\xi)_{d=0} - T_{W,0}(\xi)_{d>0} = \dot{q}_{W,0}(\xi)\frac{d}{\lambda} \tag{8a}$$

$$T_{W,f}(\xi)_{d=0} - T_{W,f}(\xi)_{d>0} = \dot{q}_{W,f}(\xi)\frac{d}{\lambda} \tag{8b}$$

Combining Eqs. (8a) and (8b),

$$[T_{W,0}(\xi) - T_{W,f}(\xi)]_{d>0} = [T_{W,0}(\xi) - T_{W,f}(\xi)]_{d=0} - \Delta\dot{q}(\xi)\frac{d}{\lambda} \tag{9}$$

$\Delta\dot{q}(\xi)$ describes the local heat flux reduction due to the application of film cooling:

$$\Delta\dot{q}(\xi) = \dot{q}_{W,0}(\xi) - \dot{q}_{W,f}(\xi) \tag{10}$$

Because of the radial arrangement of the wall thermocouples with a constant wall distance $d$, it is not possible to detect the local circumferential heat flux density $\dot{q}(\xi)$, though, for completing the correction of the film effectiveness on the chamber wall surface ($d = 0$ ), the knowledge of the local circumferential heat flux density $\dot{q}(\xi)$ is essential [see Eq. (9)]. For this reason, an averaged, non-angle-dependent heat flux density $\Delta\dot{q} = \Delta\bar{\dot{q}}(\xi)$ will be used instead to calculate the circumferential film cooling effectiveness at $d = 0$. In doing so, the resulting deviation is proportional to the circumferential temperature distribution as a first approximation with up to $\approx$10 % of the local heat flux density. To identify the circumferential averaged heat flux density $\Delta\bar{\dot{q}}(\xi)$, the results of the wall thermocouple packages next to the axial position $x/s = 280$ have been used (see also Fig. 1). Assuming a constant heat conductivity inside the liner, the local heat flux density $\dot{q}$ can be written as a function of the temperature gradient $T_{W1} - T_{W2}$, chamber radius $r$, and wall distances $d_1$ and $d_2$ (gradient method):

$$\dot{q} = \frac{\lambda}{r}\frac{T_{W1} - T_{W2}}{\ln[(r + h_2)/(r + h_1)]} \tag{11}$$

Figure 11 describes the corrected circumferential film cooling effectiveness ($d = 0$ ) as well as the measured film effectiveness ($d = 1$ mm) for the performed pressure intervals 11.5, 8, and 5 MPa, each with both film coolant blowing rates $M$ (see Table 4) for the nondimensional position $x/s = 280$ downstream the point of injection (see Fig. 1).

Consistent with the circumferential wall temperature reduction distribution with a minimum value at the angular positions of the outer coaxial injector elements ($\xi = 0$ and 36 deg) (see Fig. 9), circumferential film cooling effectiveness also shows a local minimum at these angular positions. However, maximum local film cooling effectiveness occurs at the position between the outer coaxial injector elements and film injection slots at $\xi = 18$ deg, independent of the combustion chamber pressure or the film blowing rate. Film cooling effectiveness at the upper pressure intervals 11.5 and 8 MPa show a similar behavior with a circumferential variation of about

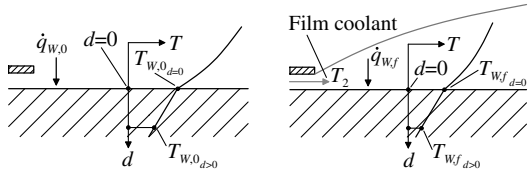


a) Without film cooling b) With film cooling

**Fig. 10 Temperature distribution and heat flux inside the combustion chamber wall.**

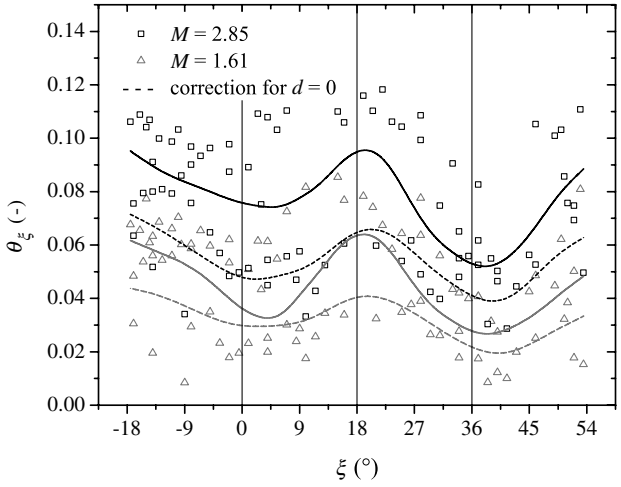


a) $p_{cc}$ = 11.5 MPa

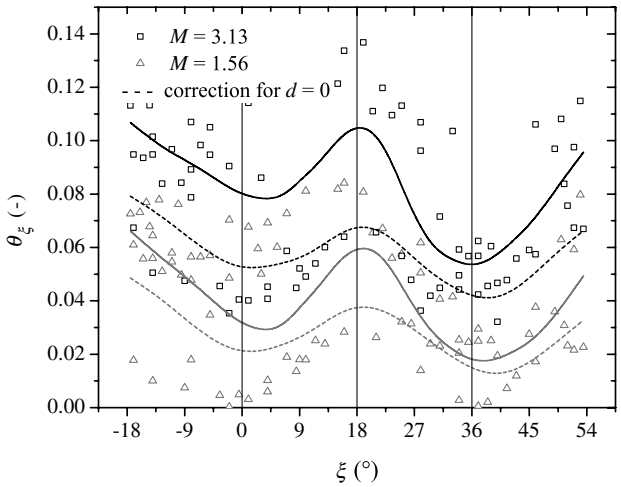


b) $p_{cc}$ = 8 MPa

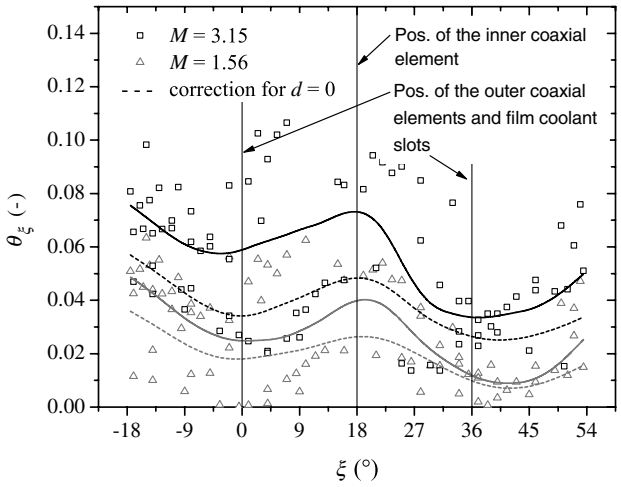


c) $p_{cc}$ = 5 MPa

**Fig. 11 Film cooling effectiveness in circumferential direction ($x/s$= 280).**

15%, whereas, for the 5 MPa, a much smaller circumferential variation of the effectiveness has been detected, especially for the lower film blowing rate [15].

Characteristics of the effectiveness, such as the positioning of maximum and minimum values in the circumferential direction, remain for the wall distance $d = 0$ [corrected film effectiveness following Eq. (9)]. However, as expected because of the assumption of a constant, non-angular-dependent local heat flux density $\bar{\dot{q}}$, a flattening of the effectiveness distribution can be observed in Fig. 11 for all pressure intervals and film blowing rates.

For analyzing the behavior of the circumferential variation of the film cooling effectiveness, the averaged variation difference $\Delta\Theta_\xi$ between the local maximum and minimum effectiveness has been used:

$$\Delta\Theta_\xi = \Theta_{\xi,\max}|_{\xi=18\,\mathrm{deg}} - \Theta_{\xi,\min}|_{\xi=0;36\,\mathrm{deg}} \tag{12}$$

Figure 12 shows the variation of the film effectiveness $\Delta\Theta_\xi$, based on the maximum effectiveness $\Theta_{\xi,\max}$, for the investigated pressure

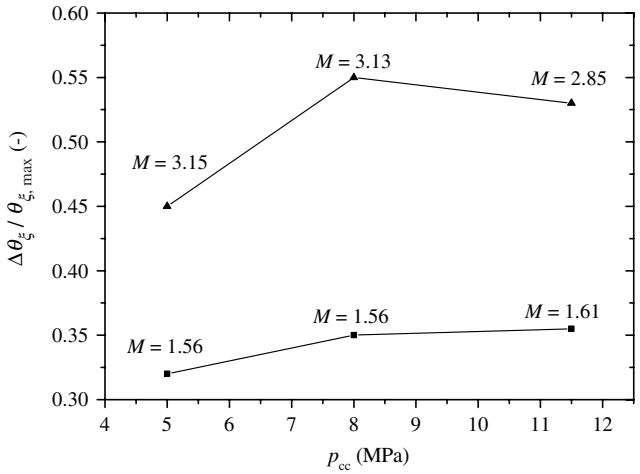


**Fig. 12 Variation of circumferential film cooling effectiveness ($d$= 1 mm, $x/s$ = 280).**

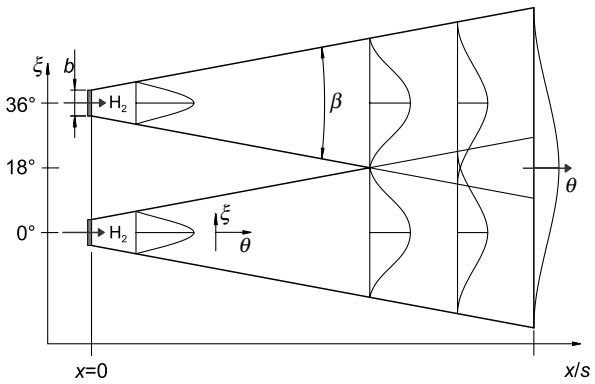


**Fig. 13 Superposition of single film cooling effectiveness.**

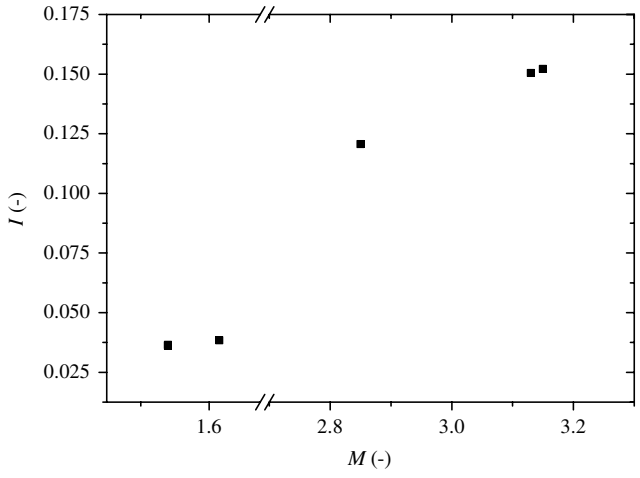


**Fig. 14 Momentum ratio in close proximity of the injector head.**

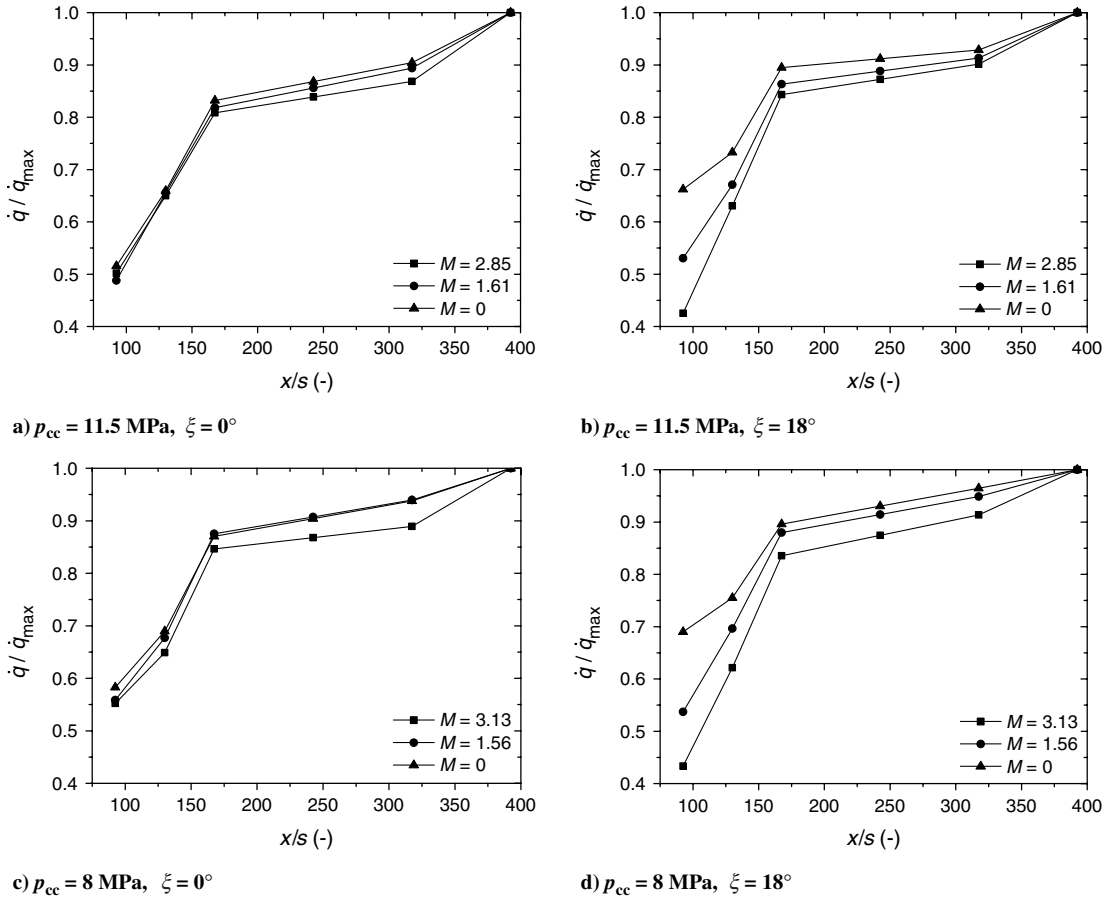


a) $p_{cc}$ = 11.5 MPa, $\xi$ = 0°

b) $p_{cc}$ = 11.5 MPa, $\xi$ = 18°

c) $p_{cc}$ = 8 MPa, $\xi$ = 0°

d) $p_{cc}$ = 8 MPa, $\xi$ = 18°

**Fig. 15 Wall heat flux distribution.**

intervals, using the results of the wall thermocouples at $x/s = 280$ with a wall distance $d = 1$ mm.

Circumferential variation is therefore not only a function of the chamber pressure, but also of the film blowing rate and the injector head design. However, results for the 11.5 and 8 MPa intervals demonstrate a very similar behavior, although the decrease at 11.5 MPa for the higher blowing rate ($M = 2.85$ ) is a result of the smaller blowing rate in comparison to the blowing rates at the other pressure intervals $M > 3$. Circumferential variation is much smaller at the 5 MPa pressure interval; an increase of the chamber pressure suppresses the even distribution of the film coolant. Furthermore, the temperature level inside the combustion chamber increases with chamber pressure and may result in a higher circumferential variation of the film cooling effectiveness.

For a constant film blowing rate, the increase of the chamber pressure is linked with a higher film mass flow rate. Using an ascertained film injection slot height $s$, it can be assumed that the boundary-layer thickness of the injected coolant stays almost constant at different combustion chamber pressure levels not too far downstream the injection. When using a higher chamber pressure, this may result in a more pronounced displacement of the film and higher heat impact of the hot gas and therefore a more distinct circumferential variation of the film effectiveness as well as the heat load distribution.

### C. Superposition of Film Cooling Effectiveness

The occurrence of the minimum film cooling effectiveness directly downstream of the film cooling slots and the maximum effectiveness of the injected film at the angular position between the slots (see Fig. 11), independent from investigated parameters like combustion chamber pressure $p_{cc}$ or film blowing rate $M$, can be explained using superposition of single slot effectiveness (see Fig. 13). Because of turbulent hot gas flow behavior and large temperature gradients between hot gas and secondary flow, comparatively intensive heating up of the injected film coolant and therefore a fast volume expansion of the coolant can be assumed. This can lead to a much higher coolant spreading angle $\beta$ in the axial direction compared with the spreading angle of a freestream jet in a nonturbulent flow. Because of the relatively high coolant spreading angle $\beta$ of the single coolant flows, downstream a certain film cooling length $x/s$ interaction and superposition of the single slot effectiveness will result in a maximum effectiveness at the angular position between the film coolant slots at $\xi = 18$ deg and minimum effectiveness at the positions $\xi = 0$ and 36 deg in the injector triangle (see Fig. 4) [36].

Besides the superposition and coolant volume expansion, the momentum flux ratio $I$ between injected propellant of an outer coaxial injector element and film coolant of a single slot, assuming uniform mass flow distribution of all injector elements and coolant injection slots, also has a certain impact on the circumferential film

**Table 6 Reproducibility of measured temperatures**

| $x/s$ | 92.5 | 130.0 | 167.5 | 242.5 | 317.5 | 392.5 |
|---|---|---|---|---|---|---|
| $T_{W,A}/T_{W,B}$ | 0.994 | 0.991 | 0.991 | 1.005 | 0.989 | 0.992 |

**Table 5 Reproducibility of hot gas conditions**

| Interval | 1 | 2 | 3 | 4 | 5 | 6 | 7 | 8 | 9 |
|---|---|---|---|---|---|---|---|---|---|
| $p_{cc,A}/p_{cc,B}$ | 0.997 | 0.996 | 0.996 | 0.996 | 0.996 | 0.998 | 0.996 | 0.996 | 0.996 |
| $ROF_A/ROF_B$ | 0.998 | 0.996 | 0.997 | 0.999 | 0.997 | 0.997 | 0.999 | 0.998 | 0.999 |

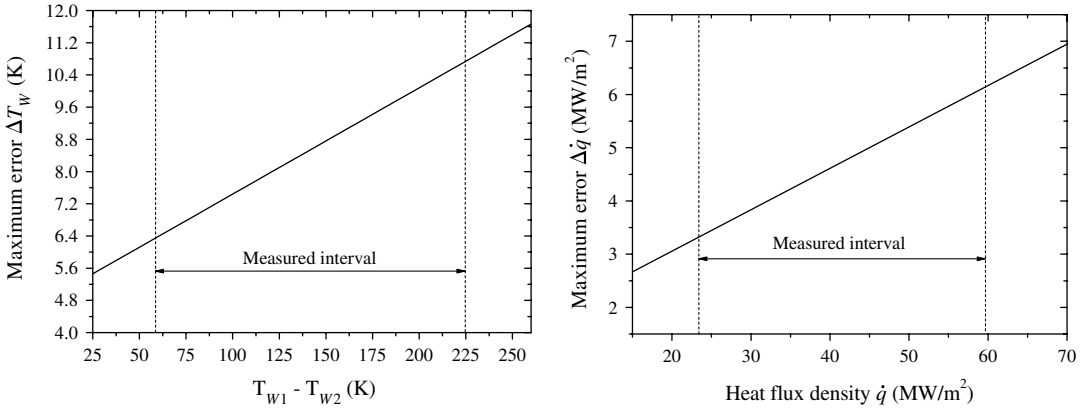


**a) Maximum wall temperature errors** **b) Maximum heat flux density errors**

**Fig. 16 Measurement errors.**

cooling effectiveness, whereas, for the injector head, the momentum flux of the LOX can be neglected in comparison with the momentum flux of the hydrogen:

$$I = \frac{(\dot{m}u)_2}{(\dot{m}u)_{H_2}} \tag{13}$$

Because of the considerably lower momentum flux of the film coolant, especially at low film blowing rates $M$, a displacement of the film mass flow because of the injector mass flow at the positions $\xi = 0$ and 36 deg in the injector triangle (see Fig. 4) toward the position between the outer coaxial elements will occur (see Fig. 14), with the result of a reduced film cooling effectiveness straight downstream of the film coolant injection slots.

### D. Circumferential Heat Flux Distribution

Figure 15 shows the normalized axial heat flux distribution $\dot{q}/\dot{q}_{\max}$ for the angular positions $\xi = 0$ and 18 deg for the upper pressure intervals 11.5 and 8 MPa. Analogous to the angular distribution of the film cooling effectiveness (see Fig. 11), the heat load reduction due to the application of a film coolant can be measured at the angular position between the outer coaxial elements and film coolant injection slots at $\xi = 18$ deg, especially in the near downstream region up to a film cooling length $x/s \approx 200$, where the influence of the film blowing rate is dominant. However, for the position $\xi = 18$ deg, only a slight influence of the film blowing rate on the film coolant related heat flux reduction can be detected. Results of the 11.5 and 8 MPa pressure intervals show very similar results for both investigated angular positions, $\xi = 0$ and 18 deg.

## V. Error Analysis

The absolute accuracy of the measured data is just as important as the reproducibility of the experiment. The heat load inside a rocket combustion chamber is predominantly driven by the combustion chamber pressure $p_{cc}$ [see Eq. (1)] and the propellant mixture ratio ROF. The comparison of two hot runs $A$ and $B$ with identical P8 test bench conditions (see Table 5) shows the excellent reproducibility of the test bench and therefore also the reproducibility of the hot gas condition inside the combustion chamber.

Comparable good results have been achieved with the measured temperatures (see Table 6 for maximum deviation at various axial positions $x/s$). The deviation of the results of the wall thermocouples is less than 2%. Assuming a hot gas side wall temperature of 800 K, the maximum fluctuation range of the local wall temperatures between two hot runs can be estimated with $\approx$15 K if worst comes to worst.

Taking into account measurement errors due to the application in the chamber wall, the following estimation can be done to judge the maximum wall thermocouple measurement errors as a function of the thermal gradient $T_{W1} - T_{W2}$ (see Fig. 16a). Maximum errors in measuring and calculating [Eq. (11)] the wall heat flux density are plotted in Fig. 16b. Finally, the following estimation can be done to judge the film cooling effectiveness errors: $\Delta\Theta \approx 0.002$–$0.025$ and $\Delta\Theta_{\bar{\xi}} \approx 0.002$–$0.025$.

In consideration of the large-scale tests with a Vulcain-2-like hot gas situation, the errors in describing temperatures, heat flux densities, and film cooling results in the subscale rocket combustion chamber are good by way of comparison.

## VI. Conclusions

Film cooling using tangential slot injection in close proximity of the coaxial injector head has been investigated for rocket-engine-like conditions with combustion chamber pressures of 11.5, 8, and 5 MPa at various film blowing rates $M$. Experimental results have shown a significant variation of circumferential wall temperature distribution and film cooling effectiveness. Minimum wall temperature reduction in the circumferential direction, independent of the combustion chamber pressure and film blowing rate, has been detected downstream of the angular positions of the outer coaxial injector elements and film injection slots. Maximum film cooling effectiveness has been measured at the angular positions of minimum wall temperature and vice versa. Circumferential variation of the film cooling effectiveness is more pronounced at higher combustion chamber pressures.

Because of the application of a film coolant, significant reduction of the wall heat flux density in the vicinity of the film coolant injection at the angular positions between the film coolant slots can be reached. For the positions directly downstream the film injection slots, only a slight reduction in wall heat flux density is visible.

Further experimental film cooling studies are planned at DLR Lampoldshausen to identify the influence of film cooling parameters like velocity ratio and slot height on circumferential film cooling effectiveness and injector-wall compatibility.

## Acknowledgment

The authors would like to acknowledge the P8 team for their assistance at the test campaign.

## References

[1] Huzel, D. K., and Huang, D. H., "*Modern Engineering for Design of Liquid-Propellant Rocket Engines*," Progress in Astronautics and Aeronautics, Vol. 147, AIAA, Washington, D.C., 1992, ISBN 1-56347-013-6.

[2] Rachuk, D. V., Gontcharov, N., and Matrinyenko, D. Y., "Evolution of the RD-0120 for Future Launch Systems," *32nd AIAA/ASME/SAE/ASEE Joint Propulsion Conference and Exhibit*, AIAA Paper 96-3004, 1996.

[3] Bartz, D. R., "A Simple Equation for Rapid Estimation of Rocket Nozzle Convective Heat Transfer Coecients," *Jet Propulsion*, Vol. 27, Jan. 1957, pp. 49–51.

[4] Sutton, G. P., "History of Liquid Propellant Rocket Engines in the United States," *Journal of Propulsion and Power*, Vol. 19, No. 6, 2003, pp. 978–1007.
doi:10.2514/2.6942

[5] Sutton, G. P., "History of Liquid-Propellant Rocket Engines in Russia, Formerly the Soviet Union," *Journal of Propulsion and Power*, Vol. 19, No. 6, 2003, pp. 1008–1037.
doi:10.2514/2.6943

[6] Popp, M., and Schmidt, G., "Rocket Engine Combustion Chamber Design Concepts for Enhanced Life," *32nd AIAA/ASME/SAE/ASEE Joint Propulsion Conference*, AIAA Paper 96-3303, 1996.

[7] Lezuo, M. L., "Wärmetransport in H2: transpirativ gekühlten Brennkammerkomponenten," Ph.D. Thesis, RWTH Aachen Univ., Aachen, Germany, 1998.

[8] Strakey, P. A., Talley, D. G., Tseng, L. K., and Miner, K. I., "Effects of Liquid-Oxygen Post Biasing on SSME Injector Wall Compatibility," *Journal of Propulsion and Power*, Vol. 18, No. 2, March–April 2002, pp. 240–246.
doi:10.2514/2.5954

[9] Fröhlke, K., Haberzettel, A., Haidn, O. J., Heinrich, S., Sion, M., and Vuillermoz, P., "First Hot Fire Test Campaign at the French-German Research Facility P8," *33rd AIAA/ASME/SAE/ASEE Joint Propulsion Conference and Exhibit*, AIAA Paper 97-2929, 1997.

[10] Arnold, R., Suslov, D., Weigand, B., and Haidn, O. J., "Investigation of Film Cooling in a High Pressure LOX/GH2 Subscale Combustion Chamber," *Space Propulsion 2008: 5th International Spacecraft Propulsion Conference & 2nd International Symposium on Propulsion for Space Transportation*, ESA/3AF/DLR Paper 42_090, 2008.

[11] "Vulcain 2 Thrust Chamber" data sheet, European Aeronautic Defence and Space Transportation GmbH, Paris, http://cs.space.eads.net/sp/PDF/vulcain2.pdf.

[12] Arnold, R., Suslov, D., Weigand, B., and Haidn, O. J., "Circumferential Behavior of Tangential Film Cooling and Injector Wall Compatibility in a High Pressure LOX/GH2 Subscale Combustion Chamber," *44th AIAA/ASME/SAE/ASEE Joint Propulsion Conference and Exhibit*, AIAA Paper 2008-5242, 2008.

[13] Suslov, D., Woschnak, A., Sender, J., and Oschwald, M., "Test Specimen Design and Measurement Technique for Investigation of Heat Transfer Processes in Cooling Channels of Rocket Engines Under Real Thermal Conditions," *24th International Symposium on Space Technology and Science ISTS*, Paper 2004-e-402004.

[14] Suslov, D., Woschnak, A., Greuel, D., and Oschwald, M., "Measurement Techniques for Investigation of Heat Transfer Processes at European Research and Technology Test Facility P8," *European Conference for Aerospace Sciences EUCASS*, Japan Aerospace Exploration Agency Paper 2004-e-40, 2004.

[15] Arnold, R., Suslov, D., and Haidn, O. J., "Experimental Investigation of Film Cooling with Tangential Slot Injection in a LOX/CH4 Subscale Rocket Combustion Chamber," *26th International Symposium on Space Technology and Science (ISTS)*, ESA Paper 2008-a-05, 2008.

[16] Wieghardt, K., "On the Blowing of Warm Air for De-Icing-Devices," (Originally, Über das Ausblasen von Warmluft für Enteiser in German), Tech. Rept., Kaiser Wilhelm-Inst. for Fluid Research, Japan Aerospace Exploration Agency Paper 2008-a-05, 2008.

[17] Hatch, J. E., and Papell, S. S., "Use of a Theoretical Flow Model to Correlate Data for Film Cooling or Heating an Adiabatic Wall by Tangential Injection of Gases of Different Fluid Properties," NASA TR D-130, 1959.

[18] Goldstein, R. J., and Haji-Sheikh, A., "Prediction of Film Cooling Effectiveness," *JSME 1967 Semi- International Symposium*, Society of Manufacturing Engineers Paper No. 225, 1967.

[19] Nishiwaki, N., Hirata, M., and Tsuchida, A., "Heat Transfer on a Surface Covered by a Cold Air Film," *International Developments in Heat Transfer*, Vol. 4, American Society of Mechanical Engineers, New York, 1961, pp. 675–681.

[20] Perez, E., *Ariane 5 User's Manual*, Issue 4, Revision 0 ed., Arianespace, Evry-Courcouronnes, France, Nov. 2004.

[21] "Vulcain 2 Nozzle" data sheet, Volvo Aero Corp., Trollhättan, Sweden, 2007.

[22] Tribus, M., and Klein, J., "Forced Convection from Nonisothermal Surfaces," *Heat Transfer Symposium*, Univ. of Michigan Press, Ann Arbor, MI, 1953.

[23] Kutateladze, S. S., and Leont'ev, A. I., "The Heat Curtain in the Turbulent Boundary Layer of a Gas," *High Temperature*, Vol. 1, No. 2, Sept.–Oct. 1963, pp. 281–290.

[24] Hartnett, J. P., Birkebak, R. C., and Eckert, E. R. G., "Velocity Distributions, Temperature Distributions, Effectiveness and Heat Transfer for Air Injected Through a Tangential Slot into a Turbulent Boundary Layer," *Journal of Heat Transfer*, Vol. 83, Aug. 1961, pp. 293–306.

[25] Ziebland, H., and Parkinson, R. C., "AGARDograph No. 148 on Heat Transfer in Rocket Engines," North Atlantic Treaty Organization, Advisory Group for Aerospace Research and Development, AGARD-AG-148-71, 1971.

[26] Goldstein, R. J., "Film Cooling," *Advances in Heat Transfer*, Vol. 7, Academic Press, New York, 1971, pp. 321–379.

[27] Stollery, J. L., and El-Ehwany, A. A. M., "A Note on the Use of a Boundary-Layer Model for Correlating Film-Cooling Data," *International Journal of Heat and Mass Transfer*, Vol. 8, No. 1, 1965, pp. 55–65.
doi:10.1016/0017-9310(65)90097-9

[28] Goldstein, R. J., Eckert, E. R. G., Tsou, F. K., and Haji-Sheikh, A., "Film Cooling with Air and Helium Injection Through a Rearward-Facing Slot into a Supersonic Air Flow," *AIAA Journal*, Vol. 4, No. 6, June 1966, pp. 981–985.
doi:10.2514/3.3591

[29] Goldstein, R. J., Rask, R. B., and Eckert, E. R. G., "Film Cooling with Helium Injection into an Incompressible Air Flow," *International Journal of Heat and Mass Transfer*, Vol. 9, No. 12, 1966, pp. 1341–1350.
doi:10.1016/0017-9310(66)90132-3

[30] Papell, S., and Trout, A. M., "Experimental Investigation of Air Film Cooling Applied to an Adiabatic Wall by Means of an Axially Discharging Slot," NASA TN D-9, Aug. 1959.

[31] Lucas, J. G., and Golladay, R. L., "An Experimental Investigation of Gaseous Film Cooling of a Rocket Motor," NASA TN D-1988, Oct. 1963.

[32] Lucas, J. G., and Golladay, R. L., "Gaseous-Film Cooling of a Rocket Motor with Injection near the Throat," NASA TN D-3836, Feb. 1967.

[33] Fissan, H. J., "Temperature Distribution in an Open Air Methane-Oxygen Flame," *Combustion and Flame*, Vol. 17, No. 3, 1971, pp. 355–358.
doi:10.1016/S0010-2180(71)80057-3

[34] Mayer, W., Schik, A. H., Vielle, B., Chauveau, C., Gökalp, I., and Talley, D., "Atomization and Breakup of Cryogenic Propellants Under High Pressure Subcritical and Supercritical Conditions," *Journal of Propulsion and Power*, Vol. 14, No. 5, 1998, pp. 835–842.
doi:10.2514/2.5348

[35] Thiard, B., "Vulcain Gas Generator Development Status," *26th SAE, ASME and ASEE Joint Propulsion Conference*, 1990, AIAA Paper 1990-2252.

[36] Goldstein, R. J., Eckert, E. R. G., Eriksen, V. L., and Ramsey, J. W., "Film Cooling Following Injection Through Inclined Circular Tubes," *Israel Journal of Technology*, Vol. 8, Nos. 1–2, March 1970, pp. 145–154.

D. Talley
*Associate Editor*